



HAL
open science

Passive monitoring of anisotropy change associated with the Parkfield 2004 earthquake

S Durand, J P Montagner, F Brenguier, R M Nadeau, Y Ricard, Philippe Roux

► **To cite this version:**

S Durand, J P Montagner, F Brenguier, R M Nadeau, Y Ricard, et al.. Passive monitoring of anisotropy change associated with the Parkfield 2004 earthquake. *Geophysical Research Letters*, 2011, 38 (13), pp.L13303. 10.1029/2011GL047875 . hal-02944873

HAL Id: hal-02944873

<https://hal.science/hal-02944873v1>

Submitted on 21 Sep 2020

HAL is a multi-disciplinary open access archive for the deposit and dissemination of scientific research documents, whether they are published or not. The documents may come from teaching and research institutions in France or abroad, or from public or private research centers.

L'archive ouverte pluridisciplinaire **HAL**, est destinée au dépôt et à la diffusion de documents scientifiques de niveau recherche, publiés ou non, émanant des établissements d'enseignement et de recherche français ou étrangers, des laboratoires publics ou privés.

Passive monitoring of anisotropy change associated with the Parkfield 2004 earthquake

S. Durand,^{1,2} J. P. Montagner,² P. Roux,³ F. Brenguier,^{2,4} R. M. Nadeau,⁵ and Y. Ricard¹

Received 21 April 2011; accepted 22 April 2011; published 7 July 2011.

[1] We investigate temporal variations in the polarization of surface waves determined using ambient seismic noise cross-correlations between station pairs at the time of the Mw 6.0 Parkfield earthquake of September 28, 2004. We use data recorded by the High Resolution Seismic Network's 3-component seismometers located along the San Andreas Fault. Our results show strong variations in azimuthal surface wave polarizations, Ψ , for the paths containing station VARB, one of the closest stations to the San Andreas Fault, synchronous with the Parkfield earthquake. Concerning the other station pair, only smooth temporal variations of Ψ are observed. Two principal contributions to these changes in Ψ are identified and separated. They are: (1) slow and weak variations due to seasonal changes in the incident direction of seismic noise; and (2) strong and rapid rotations synchronous with the Parkfield earthquake for paths containing station VARB. Strong shifts in Ψ are interpreted in terms of changes in crack-induced anisotropy due to the co-seismic rotation of the stress field. Because these changes are only observed on paths containing station VARB, the anisotropic layer responsible for the changes is most likely localized around VARB in the shallow crust. These results suggest that the polarization of surface waves may be very sensitive to changes in the orientations of distributed cracks and that implementation of our technique on a routine basis may prove useful for monitoring stress changes deep within seismogenic zones. **Citation:** Durand, S., J. P. Montagner, P. Roux, F. Brenguier, R. M. Nadeau, and Y. Ricard (2011), Passive monitoring of anisotropy change associated with the Parkfield 2004 earthquake, *Geophys. Res. Lett.*, 38, L13303, doi:10.1029/2011GL047875.

1. Introduction

[2] The impulse response of the Earth between two seismic stations s1 and s2, the so-called Green's function, can be estimated by cross-correlating ambient seismic noise signals recorded simultaneously at the two stations. The resultant correlation function represents the seismogram that

would be recorded at one of the stations, s1, if the other station, s2 were a seismic source. This property of random seismic fields has been widely studied in the past few years [Shapiro and Campillo, 2004; Wapenaar, 2004; Sabra *et al.*, 2005a]. In particular, it can be used to monitor the temporal changes of crustal properties. A recent study by Brenguier *et al.* [2008], for example, used ambient seismic noise continuously recorded by the High Resolution Seismic Network (HRSN) at Parkfield, California, (see Figure 1) to search for temporal changes in seismic velocities by computing cross-correlation functions for vertical components among all possible receiver pairs. From their analysis they found that 0.08% velocity changes occurred at the time of the September 28th, 2004 Parkfield Mw 6.0 earthquake, which they interpreted to be the result of co-seismic stress changes and damage near the San Andreas Fault (SAF). Here, we extend this investigation by considering the complete Cross-Correlation Tensor (CCT) (i.e., the nine cross-correlation functions obtained from 3-component noise records between pairs of stations) to investigate possible changes in anisotropic properties associated with this earthquake.

[3] Previous studies examining the spatial and temporal variations of seismic anisotropy in this region have been carried out using the Shear Wave Splitting (SWS) technique which refers to the splitting of a shear wave when it propagates through a cracked medium. It is completely described by the polarization direction of the leading wave and its delay time with the orthogonally polarized lagging wave [Crampin, 1987]. Liu *et al.* [2008] and Cochran *et al.* [2006] performed temporal analyses of the SWS measurements with a focus on the Parkfield seismic event and were unable to detect any precursory, co-seismic or post-seismic anisotropy change. Zhang *et al.* [2007] also produced a map of SWS anisotropy using a tomography method and found that the distribution of anisotropy in the region was relatively complex.

[4] The noise cross-correlation technique for monitoring seismic anisotropy holds several advantages over the SWS method. First, the method does not depend on the occurrence of local earthquakes for anisotropy measurements. Secondly, compared to quasi-vertically propagating shear waves used for SWS analyses, surface wave noise propagation is primarily horizontal and more directly samples horizontally-averaged seismic properties. This allows changes in the shallow crust to be more easily detected. Thirdly, the density and coverage of sampling is significantly increased, since for a seismic network of n stations all of the $n(n-1)/2$ receiver pairs can be analyzed instead of only the n receiver measurements used in SWS studies. These properties allow for very small co-seismic velocity changes to be detected [Brenguier *et al.*, 2008] and should also be beneficial for

¹Laboratoire de Géologie de Lyon, Université de Lyon 1, CNRS, Ecole Normale Supérieure de Lyon, Villeurbanne, France.

²Département de Sismologie, Institut de Physique du Globe de Paris, Paris, France.

³Laboratoire de Géophysique Interne et Tectonophysique, UMR 5559, CNRS, Saint Martin d'Hères, France.

⁴Observatoire Volcanologique du Piton de la Fournaise, La Plaine des Cafres, France.

⁵Berkeley Seismological Laboratory, University of California, Berkeley, California, USA.

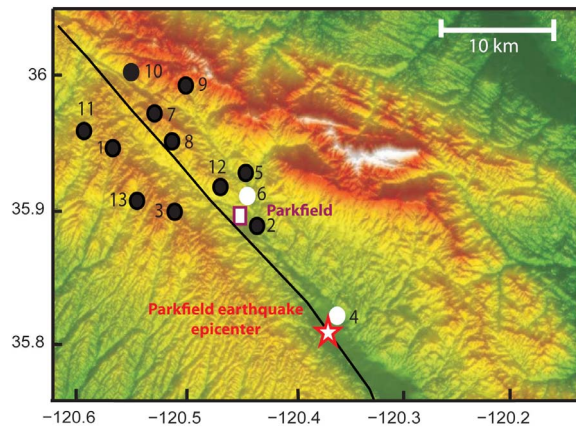


Figure 1. High-resolution seismic network map. The 13 short-period borehole seismic stations of the HRSN are shown. Only 11 short-period borehole seismic stations were used in the study (black circles) because two of them were dysfunctional at this time (white circles). These stations are distributed about the SAF (solid line). They are numbered as follows: 1, CCRB; 2, EADB; 3, FROB; 4, GHIB; 5, JCNB; 6, JCSB; 7, LCCB; 8, MMNB; 9, RMNB; 10, SCY B; 11, SMNB; 12, VARB; 13, VCAB. The red star indicates the epicenter of the 2004 Parkfield earthquake which primarily ruptured from this point to the Northwest.

studying potential anisotropy changes from the complete CCT.

2. Data Processing and Results

[5] The US Geological Survey and the State of California, USA, launched the Parkfield Prediction Experiment in the 1980's to better understand the physics of earthquakes by observing the SAF and the surrounding crust at close range before, during, and after an expected moderate earthquake [Bakun and Lindh, 1985]. The HRSN (Figure 1), consisting of a borehole (~100 to 200 m depth) seismic array of 13 stations with 3-component short-period sensors permanently cemented in place and recording at both 20 and 250 samples/s, was installed as part of this effort. In our study, HRSN data recorded over a two-year period (2004–2005) spanning the 28 September 2004 Parkfield M6.0 earthquake are used.

[6] Pre-processing of the data follows Roux [2009] (see auxiliary material for a detailed description in Figure S1) and is summarized here.¹ First, we apply spectral normalization to broaden the ambient seismic noise signal and dampen any persistent monochromatic sources within the frequency band of interest, 0.075–0.25 Hz. Second, we realize a temporal normalization of the data using a 1-bit normalization approach replacing the seismic signal by +1 when positive, and –1 when negative [Bensen et al., 2007].

[7] We then compute the nine-components of the CCT for the 78 receiver pairs of the HRSN array for the time period 2004–2005. For each station pair $\{i, j\}$, we define a seismic coordinate system, (R, T, Z), relative to the great-circle-path

joining the pair, and all components of the CCT are calculated according to:

$$[C_{ij}(t)]_{kl} = \frac{\int_0^{\tau_0} S_{ik}(\tau) S_{jl}(t + \tau) d\tau}{\sqrt{\int_0^{\tau_0} S_{ik}^2(\tau) d\tau \int_0^{\tau_0} S_{jl}^2(\tau) d\tau}} \quad (1)$$

where i or $j = \{1, 2, \dots, 13\}$ refers to the station numbering, k or $l = \{R, T, Z\}$ to the ambient noise component, $(C_{ij})_{kl}$ to the CCT components calculated for a duration τ_0 of 120 s and S to a seismic trace filtered between 0.075 and 0.25 Hz. We then stack the cross-correlation functions over 30 days to improve the signal-to-noise ratio, to provide stable waveforms, and to converge on the actual Green's function (see Figure S2). However, this stacking also limits the temporal resolution of our analysis to ~30-days.

[8] An example of CCT is shown in Figure 2 (top). Here, energy is present on all 9 CCT components and the CCT is not symmetric. For an isotropic homogeneous medium with a random distribution of noise source the TZ, ZT, TR and RT CCT-components are expected to be, on average, zero. The presence of non zero components is due either to the presence of anisotropy, heterogeneities or to a non isotropic distribution of noise [Roux, 2009]. We now successively discuss these two possibilities.

[9] In a weakly anisotropic and/or heterogeneous medium, the polarization directions (R,T,Z) related to the great-circle-path joining a given station pair are slightly shifted to new ones (R',T',Z') so that the T'Z', Z'T', TR' and RT' CCT-components no longer cancel (Figure 2, bottom). The resulting waves are called quasi-Rayleigh and quasi-Love waves [Crampin, 1975]. The polarization directions of the quasi-surface waves can be obtained by searching for each receiver pair, the orientation of each seismic station, i.e., computing a new appropriate coordinate system R', T', Z', that minimizes the energy present on the RT', T'R', ZT' and T'Z' tensor components (Figure 2, top). This is done automatically using the Optimal Rotation Algorithm (ORA) [Roux, 2009] where two rotations for each station i of a receiver pair, around the vertical and the radial axes, are used to define, respectively, an azimuth Ψ and a tilt δ (Figure 2, bottom).

[10] In the case of a biased noise sources distribution, the TZ, ZT, TR and RT CCT-components can also be non-zero. The same ORA algorithm reveals in this case the main direction of the incoming noise as the CCT only provides information on the surface-wave contribution to the Green's function projected along the incident noise direction [Roux, 2009].

[11] We analysed all the data for the time period (2004–2005). For each station pair, a misfit parameter is also calculated to evaluate the quality of the optimization and is defined as the ratio of the residual energy on the RT, TR, ZT and TZ tensor components, after rotation, divided by the total energy of the tensor. We consider the optimization satisfactory when the misfit is less than 5% of the total energy remaining on the RT, TR, ZT and TZ components. This rigorous selection criteria ensures that only the best rotated CCTs are used in the subsequent analysis. We also confirmed that all selected stations were operating properly

¹Auxiliary materials are available in the HTML. doi:10.1029/2011GL047875.

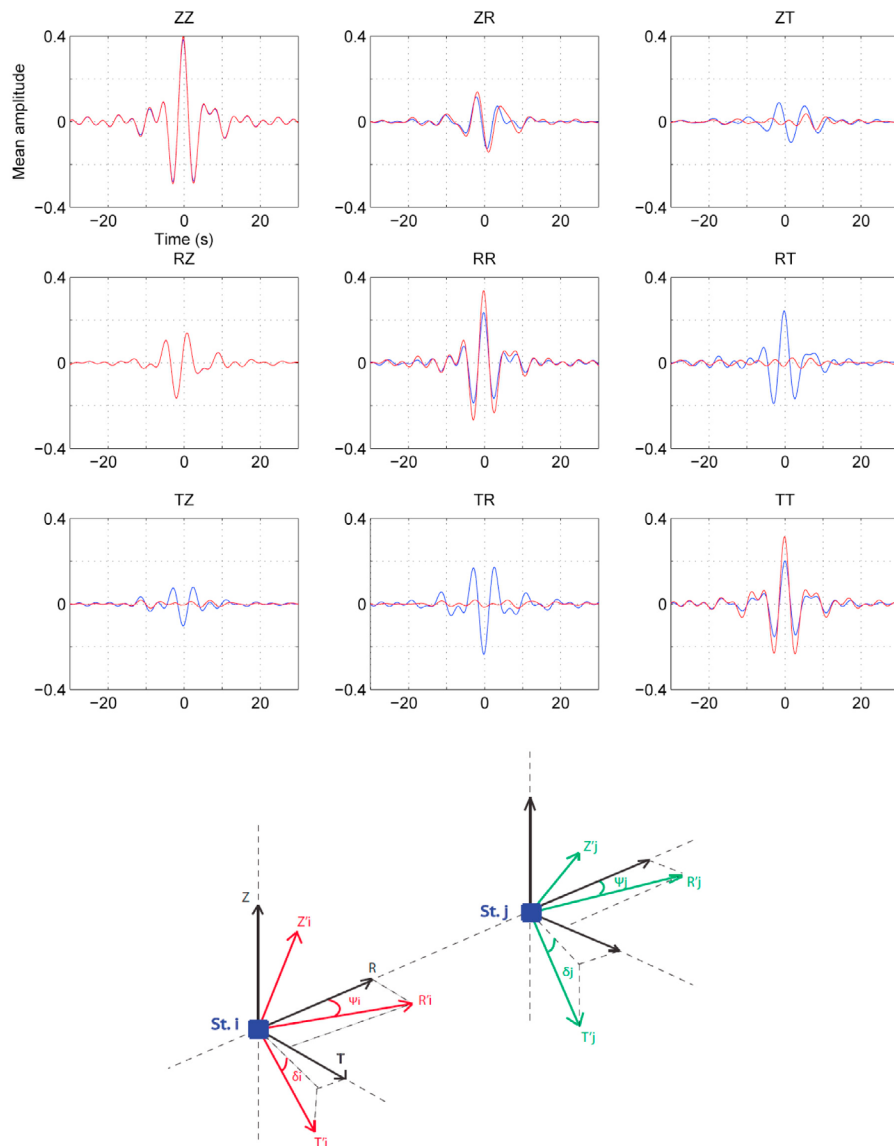


Figure 2. (top) An example of a CCT averaged over 30 days before and after the optimal rotation algorithm for the receiver pair 1–11 (CCRB-SMNB). The CCT was calculated from pre-processed ambient seismic noise data recorded at station receivers 1 (CCRB) and 11 (SMNB) (blue curves). Energy is present on all components, which means that the Rayleigh and Love waves are not aligned with the noise incidence direction in their initial coordinate seismic system and/or are propagating in an anisotropic and/or heterogeneous medium. After the ORA, the re-alignment of the stations results in a correlation tensor with a quasi-Rayleigh and a quasi-Love wave (red). (bottom) Azimuths Ψ and tilts δ used in the optimal rotation algorithm.

in the frequency band of interest during the critical period spanning the Parkfield earthquake.

[12] Temporal variations in Ψ are small, except for the receiver pairs that include station 12 (VARB), for which a significant synchronous co-seismic jump is observed (see Figure S3, bottom). Concerning the tilt δ , changes are always small (within $\sim \pm 5^\circ$). This contrast is in agreement with the response to co-seismic stress change expected for Ψ and δ in the tectonic environment of the SAF where the stress field is dominated by horizontal forces [e.g., *Boness and Zoback, 2006*]. However, before relating these variations to anisotropy changes, we must discuss the effects of

noise directivity and noise incidence temporal changes on Ψ and δ .

[13] We performed beamforming measurements using data from the entire HRSN array to obtain the noise incidence angle and the phase velocity for periods between 5s and 10s. Beamforming was performed using the N stations of HRSN:

$$B(\theta, c) = \frac{1}{\Delta\omega} \int_{\omega_c - \Delta\omega/2}^{\omega_c + \Delta\omega/2} \left| \sum_{i=1}^N \tilde{S}_i(\omega) \exp \left[i \frac{\omega}{c} (x_i \sin \theta + y_i \cos \theta) \right] \right|^2 d\omega \quad (2)$$

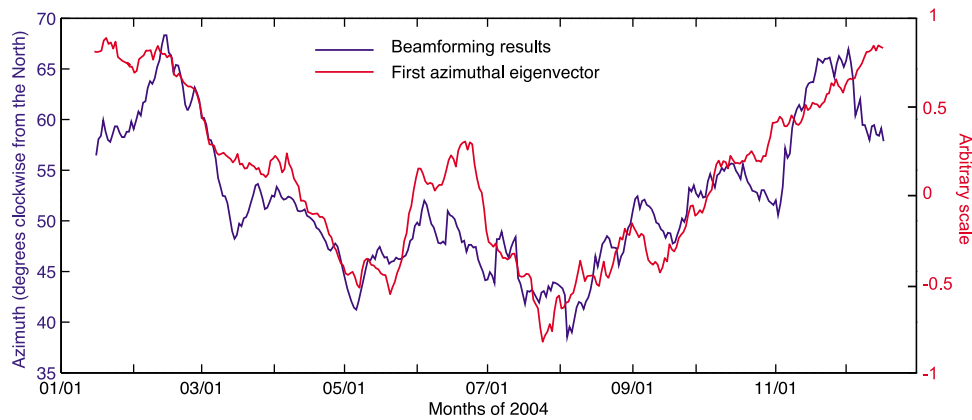


Figure 3. Seasonal contribution to the azimuthal temporal variations compared with the beamforming results. Seismic noise incidence angle through 2004, determined by beamforming on the seismic network, with a 30-day average (blue curve). First eigenvector of the azimuth (arbitrary amplitude, red curve). Their similarities confirm that the azimuth records the temporal variations of the seismic noise incidence angle.

where $\tilde{S}_i(\omega)$ is the frequency spectrum of the signal at station i , ω the frequency, θ the incidence angle of the seismic noise, c the group velocity, $\Delta\omega$ the frequency bandwidth, ω_c the central frequency and (x_i, y_i) the spatial coordinates of station i . Similar to the results of *Stehly et al.* [2006], we find that ambient noise comes primarily from Pacific Ocean, with incidence angles varying between 40° and 70° clockwise from North (Figure 3, blue curve). Rapid temporal changes in the principal direction of incidence of the noise source could potentially be responsible for significant contributions to the temporal changes seen in the noise CCT.

[14] To remove contributions to the temporal signal that are dependent on the incidence of the noise source, we performed a Singular Value Decomposition (SVD) on the matrix M of temporal azimuthal variations for the best station pairs, with M having the dimensions of number of the

best stations pairs by the number of days. The SVD transforms M into the product of three matrices denoted U , S and V such that $M = U*S*V^t$. Here the exponent “t” indicates transposition of the matrix, S is the diagonal matrix of the singular values, U is the matrix of the station eigenvectors and V is the matrix of the temporal eigenvectors. V contains information on the different contributions to the temporal changes in polarization. The first eigenvector of V shows slow and weak annual variations, similar with the beamforming signal (Figure 3). Moreover, it does not display the observed strong and rapid temporal variations at the time of the Parkfield earthquake. This result confirms that temporal changes in the noise source’s incidence direction can have impact on the observed variations in polarization. We can remove this dependence from the matrix M by setting the first azimuthal eigenvalue to 0 (i.e., by ignoring

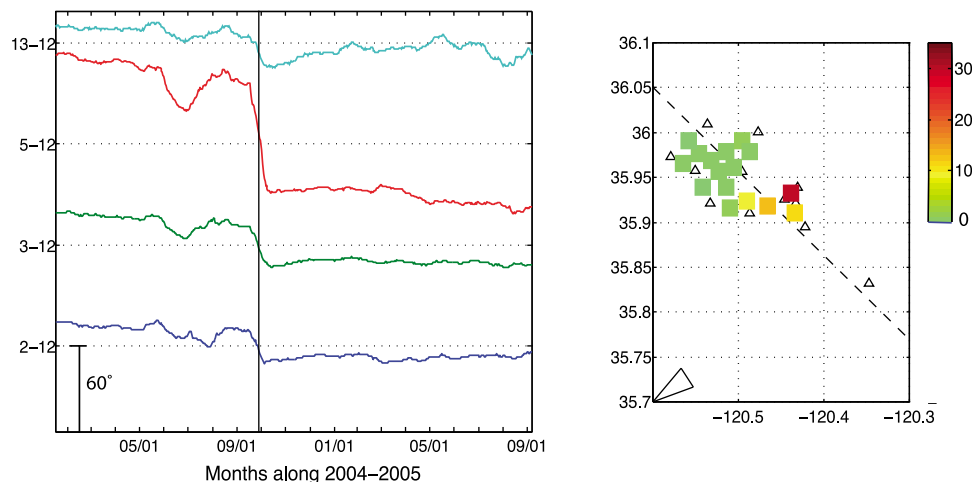


Figure 4. (left) Temporal variations of the azimuth observed at station 12 (VARB) for the best receiver pairs involving this station, after removing the directivity dependent seasonal noise contribution. A synchronous co-seismic azimuthal jump is observed. Vertical black line is time of the Parkfield earthquake. (right) Map of the absolute azimuthal variations at the moment of the Parkfield earthquake, averaged between both station of each best selected receiver pair (misfit less than 5%). We plotted the amplitude of the absolute temporal variations in azimuth mid-way between the receiver pairs. The colorbar gives the amplitude scale of the azimuth change in degrees. The four southeast points are those of the receiver pairs containing station 12. Note that the strong and fast azimuthal co-seismic changes occur only within a precise zone in the southeastern portion of the seismic array, near the SAF, and above the primary rupture zone of the Parkfield earthquake.

this eigenvector) and reconstructing M with the remaining eigenvectors.

[15] Figure 4 (left) shows the results of this process at station 12 for the best selected receiver pairs containing this station, and the strong co-seismic jumps in Ψ are still observed. Temporal variations of Ψ for all low misfit receiver pairs, both before and after their noise correction, are shown in Figures S3 (bottom) and S3 (top), respectively. These results demonstrate that the slowly varying temporal changes of polarization related to seasonal variations in source noise directivity are uncorrelated with the rapid and stronger variations occurring at the time of the Parkfield earthquake.

[16] A map representation of the absolute azimuthal variations at the moment of the Parkfield earthquake, averaged between both station i and j of station pair (i, j) (i.e., $[|\Psi_i(t_2) - \Psi_i(t_1)| + |\Psi_j(t_2) - \Psi_j(t_1)|]/2$ where t_1 and t_2 refers respectively to before and after the Parkfield earthquake), for all the selected receiver pairs is given in Figure 4 (right). The color symbols depicting these variations are plotted mid-way of the station pairs. It is clear that the variations are almost zero for station pairs which do not include station 12 (VARB), while the strong and rapid variations are observed at a specific location, South East end of the seismic array, over the rupture zone of the Parkfield earthquake and where the receiver pairs containing station 12 are located.

3. Discussion

[17] Our seismic noise cross-correlation method combined with ORA analysis has revealed strong co-seismic changes in quasi-surface wave azimuthal polarization for paths containing station 12, located over the rupture zone of the 2004 Parkfield earthquake. This station (VARB) is also one of the closest stations to the SAF (Figure 1). Therefore, the observed co-seismic changes are likely to be a local effect in a small area surrounding station 12 (Figure 4, right). Roux *et al.* [2005] showed that the Rayleigh wave velocity in the Parkfield area varies from 1000 to 3000 m/s in the 0.075-0.25 Hz frequency range used in this study. This suggests that we are sensitive to changes taking place at depths down to approximately 20 km (one-half of the wavelength). However, an examination of the depth sensitivity of Rayleigh waves [Dahlen and Tromp, 1998, p. 449] shows they are also particularly sensitive to physical properties in the upper 3 km. Hence if any velocity perturbations occur at depths where the sensitivity is maximum, they should have a measurable effect on their amplitude. For this reason, we interpret the changes to be related to crustal damage occurring at least in the upper 3 km, and potentially deeper down to the middle lower crust. This interpretation also does not contradict results of other recent studies of anisotropy derived from SWS along the SAF [Cochran *et al.*, 2006; Liu *et al.*, 2008], because we believe our observed changes result from propagation through a thin anisotropic layer of limited extent, a case that was not addressed by these previous studies.

[18] Liu *et al.* [2006] reported that very strong local site amplification exists in the vicinity of station 12. They interpreted this to be the result of the presence of a low velocity fault-zone conductor [Leary and Ben Zion, 1992] believed to be a zone of fractured rock with high pore-fluid pressure

capable of amplifying seismic waves. If true, it is not so surprising that station 12 corresponds to the area where the strongest temporal variations of the physical parameters are observed. Studies of other fault systems have also reported strong temporal changes in seismic properties using other methods (e.g., Wu *et al.* [2009] for the north Anatolian fault in Turkey).

[19] Crack induced anisotropy [Crampin, 1987] provides a simple model to explain these temporal changes. In this model, cracks open and close during the strong shaking associated with an earthquake in response to the co-seismic rotation of the stress field. Because crack density decreases with depth and lithostatic pressure increases with depth, it is likely to occur in the first 5 km, where surface waves are also very sensitive. Additional evidence supporting crack activity during the Parkfield earthquake comes from Li *et al.* [2007] who reported the occurrence of significant rock damage and healing related to the mainshock of the Parkfield earthquake and Rubinstein and Beroza [2005] who explained their observed travel-time delays in the S coda before and after the Parkfield earthquake by the opening of cracks during the mainshock. These types of observations are not limited to the SAF at Parkfield. Indeed, for the Loma Prieta earthquake in 1989, Baisch and Bokelmann [2001] proposed co-seismic deformation and crack opening mechanisms from localized shear stress or pore-fluid pressure changes to explain their observations, and Tadokoro *et al.* [1999] reported temporal changes in crack-induced anisotropy near the Nojima fault due to the magnitude 7.2, 1995, Kobe earthquake.

[20] The noise technique is more sensitive to temporal changes in azimuthal polarization than the SWS method. Consider, for example, the case where anisotropy related to the rotation of the stress field affects the orientation of a distribution of cracks in a given anisotropic layer. As a first-order approximation, the crack distribution in this layer, in the context of SAF tectonics, can be modeled as a transversely isotropic medium with a horizontal axis of symmetry and with anisotropy of a few percent. In this case the time delay $\frac{\delta t}{t}$ related to this thin layer only, for an incident surface wave with an azimuth ψ is:

$$\begin{aligned} \frac{\delta t}{t} &= -\frac{\delta v}{v} \approx A\{\cos[2(\Psi - \Psi_{\alpha 1})] - \cos[2(\Psi - \Psi_{\alpha 2})]\} \\ &= 2A \sin(2\Psi - \Psi_{\alpha 1} - \Psi_{\alpha 2}) \sin(\Psi_{\alpha 1} - \Psi_{\alpha 2}) \end{aligned} \quad (3)$$

where A is the anisotropy amplitude in the anisotropic layer, $\Psi_{\alpha 1}$ and $\Psi_{\alpha 2}$, is the anisotropy direction before and after the earthquake [Montagner and Nataf, 1986]. Considering a change of anisotropy from 0 to 25 degrees seen by a wave propagating with an azimuth of $\Psi = 0$ in a medium with 3% anisotropy, circumstances that should be easily detected by our method, leads to a relative time delay $\delta t/t$ of 1% and to an absolute time delay of only 5 ms per km of anisotropic layer. Therefore, such a variation over a thin layer of 5 km would not be detected by SWS technique. Additional numerical tests will be necessary to better understand how our observations relate to these other measures of temporal change and changes in physical properties of the fault zone.

[21] In conclusion we feel that in a crack opening and closing environment, the polarization of surface waves is a more sensitive parameter for the measurement of temporal

changes when compared to travel times measurements. There is also clearly the potential to implement our new approach on a routine basis for the purpose of continuously monitoring stress changes in seismogenic zones.

[22] **Acknowledgments.** The High-Resolution Seismic Network is operated by the Berkeley Seismological Laboratory, University of California, USA, with financial support from the US Geological Survey through awards 07HQAG0014 and G10AC00093. We would like to thank Richard Allen and the two reviewers for their critical reading and their suggestions, which helped us to improve the quality of this paper.

References

- Baisch, S., and G. H. R. Bokelmann (2001), Seismic waveform attributes before and after the Loma Prieta earthquake: Scattering change near the earthquake and temporal recovery, *J. Geophys. Res.*, *106*, 16,323–16,337, doi:10.1029/2001JB000151.
- Bakun, W. H., and A. G. Lindh (1985), The Parkfield, California, earthquake prediction experiment, *Science*, *229*, 619–624, doi:10.1126/science.229.4714.619.
- Bensen, G. D., M. H. Ritzwoller, M. P. Barmin, A. L. Levshin, F. Lin, M. P. Moschetti, N. M. Shapiro, and Y. Yang (2007), Processing seismic ambient noise data to obtain reliable broad-band surface wave dispersion measurements, *Geophys. J. Int.*, *169*, 1239–1260, doi:10.1111/j.1365-246X.2007.03374.x.
- Boness, N. L., and M. D. Zoback (2006), Mapping stress and structurally controlled crustal shear velocity anisotropy in California, *Geology*, *34*, 825–828, doi:10.1130/G22309.1.
- Brenguier, F., M. Campillo, C. Hadziioannou, N. M. Shapiro, R. M. Nadeau, and E. Larose (2008), Postseismic relaxation along the San Andreas Fault at Parkfield from continuous seismological observations, *Science*, *321*, 1478–1481, doi:10.1126/science.1160943.
- Cochran, E., Y. G. Li, and J. Vidale (2006), Anisotropy in shallow crust observed around the San Andreas fault before and after the 2004 M 6.0 Parkfield earthquake, *Bull. Seismol. Soc. Am.*, *96*, S364–S375, doi:10.1785/0120050804.
- Crampin, S. (1975), Distinctive particle motion of surface waves as a diagnostic of anisotropic layering, *Geophys. J. R. Astron. Soc.*, *40*, 177–186.
- Crampin, S. (1987), Geological and industrial implications of extensive-dilatancy anisotropy, *Nature*, *328*, 491–496, doi:10.1038/328491a0.
- Leary, P., and Y. Ben Zion (1992), A 200m wide fault zone low velocity layer on the San Andreas Fault at Parkfield: Results from analytic waveform fits to trapped wave groups, *Seismol. Res. Lett.*, *63*, 62.
- Li, Y. G., P. Chen, E. S. Cochran, and J. E. Vidale (2007), Seismic velocity variations on the San Andreas fault caused by the 2004 M6 Parkfield Earthquake and their implications, *Earth Planets Space*, *59*, 21–31.
- Liu, P., S. Custodio, and R. Archuleta (2006), Kinematic inversion of the 2004 M 6.0 Parkfield earthquake including an approximation to tsite effects, *Bull. Seismol. Soc. Am.*, *96*, S143–S158, doi:10.1785/0120050826.
- Liu, Y., H. Zhang, C. Thurber, and S. Roecker (2008), Shear wave anisotropy in the crust around the San Andreas fault near Parkfield: Spatial and temporal analysis, *Geophys. J. Int.*, *172*, 957–970, doi:10.1111/j.1365-246X.2007.03618.x.
- Montagner, J. P., and H.-C. Nataf (1986), A simple method for inverting the azimuthal anisotropy of surface waves, *J. Geophys. Res.*, *91*, 511–520, doi:10.1029/JB091iB01p00511.
- Roux, P. (2009), Passive seismic imaging with directive ambient noise: Application to the San Andreas Fault (SAF) in Parkfield, *Geophys. J. Int.*, *179*, 367–373, doi:10.1111/j.1365-246X.2009.04282.x.
- Roux, P., K. G. Sabra, P. Gerstoft, W. A. Kuperman, and M. C. Fehler (2005), P-waves from cross-correlation of seismic noise, *Geophys. Res. Lett.*, *32*, L19303, doi:10.1029/2005GL023803.
- Rubinstein, J., and G. C. Beroza (2005), Depth constrain on nonlinear strong ground motion from the 2004 Parkfield earthquake, *Geophys. Res. Lett.*, *32*, L14313, doi:10.1029/2005GL023189.
- Sabra, K. G., P. Gerstoft, P. Roux, W. A. Kuperman, and M. C. Fehler (2005a), Extracting time-domain Green's function estimates from ambient seismic noise, *Geophys. Res. Lett.*, *32*, L03310, doi:10.1029/2004GL021862.
- Shapiro, N. M., and M. Campillo (2004), Emergence of broadband Rayleigh waves from correlations of the ambient seismic noise, *Geophys. Res. Lett.*, *31*, L07614, doi:10.1029/2004GL019491.
- Stehly, L., M. Campillo, and N. M. Shapiro (2006), A study of the seismic noise from its long-range correlation properties, *J. Geophys. Res.*, *111*, B10306, doi:10.1029/2005JB004237.
- Tadokoro, K., M. Ando, and Y. Umeda (1999), S-wave splitting in the aftershock region of the 1995 Hyogo-ken earthquake, *J. Geophys. Res.*, *104*, 981–991, doi:10.1029/1998JB900024.
- Wapenaar, K. (2004), Retrieving the elastodynamic Green's function of an arbitrary inhomogeneous medium by cross correlation, *Phys. Rev. Lett.*, *93*, 254301, doi:10.1103/PhysRevLett.93.254301.
- Wu, C., Z. Peng, and Y. Ben Zion (2009), Non-linearity and temporal changes of fault zone site response associated with strong ground motion, *Geophys. J. Int.*, *176*, 265–278, doi:10.1111/j.1365-246X.2008.04005.x.
- Zhang, H., Y. Liu, C. Thunber, and S. Roeker (2007), Three-dimensional shear-wave splitting tomography in the Parkfield, California, region, *Geophys. Res. Lett.*, *34*, L24308, doi:10.1029/2007GL031951.
- F. Brenguier, Observatoire Volcanologique du Piton de la Fournaise, 14 RN3 - Km 2.7, F-97418 La Plaine des Cafres CEDEX, France.
- S. Durand and Y. Ricard, Laboratoire de Géologie de Lyon, Université de Lyon I, CNRS, Ecole Normale Supérieure de Lyon, 2 rue Raphaël Dubois, F-69622 Villeurbanne CEDEX, France. (stephanie.durand@ens-lyon.fr)
- J. Montagner, Département de Sismologie, Institut de Physique du Globe de Paris, 1 rue Jussieu, Etage 3, F-75238 Paris CEDEX 05, France.
- R. M. Nadeau, Berkeley Seismological Laboratory, University of California, 215 McCone Hall, Berkeley, CA 94760, USA.
- P. Roux, Laboratoire de Géophysique Interne et Tectonophysique, UMR 5559, CNRS, Maison des Géosciences, 1381 rue de la Piscine, F-38400 Saint Martin d'Hères CEDEX, France.